J. Chem. Sci. Vol. 126, No. 3, May 2014, pp. 659–675.

Study of structure and spectroscopy of water–hydroxide ion clusters: A combined simulated annealing and DFT-based approach

SATYAJIT GUHA, SOUMYA GANGULY NEOGI and PINAKI CHAUDHURY*
Department of Chemistry, University of Calcutta, 92, APC Road, Kolkata 700 009, India
e-mail: pinakc@rediffmail.com

MS received 7 June 2013; revised 18 November 2013; accepted 4 December 2013

Abstract. In this paper, we explore the use of stochastic optimizer, namely simulated annealing (SA) followed by density function theory (DFT)-based strategy for evaluating the structure and infrared spectroscopy of $(H_2O)_n\,OH^-$ clusters where $n = 1$–6. We have shown that the use of SA can generate both global and local structures of these cluster systems. We also perform a DFT calculation, using the optimized coordinate obtained from SA as input and extract the IR spectra of these systems. Finally, we compare our results with available theoretical and experimental data. There is a close correspondence between the computed frequencies from our theoretical study and available experimental data. To further aid in understanding the details of the hydrogen bonds formed, we performed atoms in molecules calculation on all the global minimum structures to evaluate relevant electron densities and critical points.

Keywords. Simulated annealing; density function theory; water clusters; infrared spectrum.

1. Introduction

Cluster chemistry and physics have become an actively pursued area of research in contemporary chemical physics. Both atomic and molecular clusters are studied and characterized with great effort. Experimentalists are interested in determining the bonding,[1–18] structure and spectroscopy of these systems and theoreticians have contributed to the logical explanation of experimental findings. There are different types of systems ranging from atomic clusters, especially noble gas clusters (modelled by Lennard Jones (LJ) potential), metallic and alloy clusters (modelled by Gupta potential) and molecular clusters, especially water clusters (modelled by ST2, SPC, TIP2P, BF, TIPS2, TIP3P, TIP4P, SPCE/POL, etc.) and hydrated halide ion clusters (modelled by modified TIP3P, TIP4P, SPCE/POL, etc.), which are studied extensively by different researchers.[19–40] These potentials are a combination of Lennard–Jones and Coulombic interactions with the contribution of polarizability factors. Besides these model potentials, theoreticians have also used brute force *ab initio* based quantum chemical calculations using DFT, MP2, etc. on these systems.[41–96] Still the size-specific water-hydroxide ion clusters where water encapsulates a single hydroxide ion is an interesting system and a principal subject for molecular dynamics and statistical mechanical simulations.

The study of these cluster systems using the above mentioned empirical potentials is difficult because the potential energy surface (PES) of these systems is extremely rugged and supports multiple minima. The task of finding the global or the deeper minima in these systems is challenging and can be a serious test of different optimization techniques. In scenarios such as these, it is prudent to switch over to stochastic optimization techniques against conventional deterministic ones. The reason is obvious. Stochastic techniques have a greater potential of finding global minimum than deterministic ones. Simulated annealing (SA)[97–117] is one such celebrated scheme and has been widely used in contemporary chemical studies and can be a good choice for studying hydrogen bonded[118–122]cluster systems of the type $(H_2O)_n\,OH^-$ as shown by us.

The motivation for studying these systems is manifold. The most obvious is to see how competing hydrogen bonds and their relative strengths dictate the final structure that a cluster such as these can have. The generation of size specific clusters and the characterization of the O – H stretching frequencies for water molecules coordinating hydroxide ion as well as its variation with the size of the cluster is an engaging area of research. If the central ion is OH^-, one of the possible hydrogen bonded interactions is of $O - H - - - OH^-$ type. In

*For correspondence

this situation, one might expect that the ultimate structure of a given $(H_2O)_n\,OH^-$ cluster will be dictated by the creation of as many $O-H---OH^-$ interactions as possible. In such cluster systems, there might arise a situation when after arranging a certain number of O – H bonds of H_2O towards hydroxide (OH^-), a saturation point is reached and any excess H_2O molecule added to the cluster system will form hydrogen bonded network to other water molecules, the interaction being of O−H−−−O type. These hydrogen bonds also leave their mark on the infrared (IR) spectroscopy of these systems. The general trend is the occurrence of intensified red-shifted peaks compared to the position of the O – H stretch in free water. Cages formed by O−H−−−O interaction show their signature on the infrared (IR) spectroscopy of these systems also. This study propose and use a combined SA+DFT strategy to find out high quality structures as well as IR spectroscopic modes. We believe that an initial search on an empirical PES by SA followed by a DFT calculation using the optimized SA structure can lead to the achievement of good quality structures with comparatively reduced computational labour. As a check on the quality of the structure evaluated, spectroscopic modes are determined and the results compared with those available in literature.

2. Experimental

2.1 *Potential for the system*

To model the $(H_2O)_n\,OH^-$ cluster system, we have used intermolecular potential function known as TIP3P as suggested by Jorgensen *et al.* [19–21] It is a combination of Lennard Jones and electrostatic or coulomb terms which acts between all intermolecular pairs of charges. The model consists of a rigid water monomer which has three interaction sites. Here, the LJ potentials are present between oxygen atoms. Besides this, the model has charge separation for which it possesses a negative charge ($-0.834e$) on oxygen and positive charge ($0.417e$) on hydrogen and to accommodate excess negative charge, the charge on oxygen of OH^- ion is $-1.417e$. Total potential energy expression for the cluster system can be written as

$$U_{\text{total}} = U_{\text{LJ}} + U_{\text{coul}}, \tag{1}$$

where U_{LJ} is the Lennard Jones interaction energy and U_{coul} is the coulombic interaction energy. Detailed expressions of the potential energy are given in the paper by Jorgensen *et al.*[19–21] The parameters for the potential function are given in table 1. It must be mentioned, here that other models for water clusters exist, which incorporate more interactions over TIP3P such as SPCE/POL or TIP4P. We perform our initial evaluation of structures using SA with the TIP3P potential because our strategy ultimately is to perform a DFT calculation with the pre-optimized SA structures. Since the TIP3P-supported structures will be further verified at the DFT level, we desist from using other models such as the SPCE/POL or TIP4P.

Table 1. Potential energy parameters used in model potential.

Parameters for potential energy function	
r(OH), Å	0.9572
∠HOH, deg	104.52
A × 10^{-3}, kcal Å^{12}/mol	582.0
C, kcal Å^6/mol	595.0
q(O)	−0.834
q(H)	0.417

2.2 *Simulated annealing method*

After generating potential energy for the system, we use stochastic global optimizer called simulated annealing to determine the critical points which are supported by the potential energy function and ultimately determine structures of the water–hydride clusters. SA is a technique which borrows its working principle from the physical process of annealing. In physical annealing, a moistened melt of metal is heated to a very high temperature and then cooled down very slowly to reach the thermodynamic minimum energy state. The origin of the working of SA is based on metropolis sampling scheme. If find out the minima (global and local) of a potential energy function, one has to start with a randomly generated and guessed solution. This solution is far away from the actual solution. Here, one needs to modify the starting solution using some criteria so that at the end, the desired minimum (global and local) solution is found out. The solution with which the process is started can be updated in the following way, for the initial set, one coordinate is randomly selected say y_k^0. Then, a random change is given in the following way,

$$y_k^1 = y_k^0 + (-1)^i\,\Delta R. \tag{2}$$

In eq. (2), i is a random integer, R is a random number (between 0 and 1) and Δ is the desired amplitude of change. Now, the variable can change in both the positive and negative direction. After obtaining the new set of coordinates, one can calculate U_{total}^1 where U_{total}^1 is the total potential energy from the new set.

The U^1_{total} is evaluated by using the updated coordinates and eq. (1) to calculate the energy of the instantaneous structures at the TIP3P level of theory. The value of U^1_{total} can be compared with the potential energy U^0_{total}, which is evaluated with the older set of coordinates. The move is accepted when $U^1_{\text{total}} < U^0_{\text{total}}$ and if the reverse occurrs, the move is not rejected directly and it is subjected to the Metropolis Sampling Test. Now we have constructed a function, generally known as objective function (F)

$$F = (U_{\text{total}} - U_{\text{L}})^2 , \tag{3}$$

where U_{L} is lower bound energy and its value is supplied. Through the search, the value of F will be minimized and it is obtained when U_{total} is minimized. With U^0_{total}, F^0 is evaluated and with U^1_{total}, F_1 is evaluated. Now, if $\Delta F(F_1 - F_0)$ is negative, the move is accepted, otherwise it is subjected to the Metropolis Sampling Test.

In SA, there is a temperature-like quantity (T_{at}), which is similar to annealing temperature at every step. It helps to evaluate the sampling probability, which is

$$P_{\text{S}} = \exp\left(\frac{-\Delta F}{T_{\text{at}}}\right). \tag{4}$$

The value of P_{S} is in between 0 and 1. A random number R which is also in between 0 and 1 is called and it is compared with P_{S}. If P_{S} is larger than R, the move is accepted, otherwise it is rejected. In the initial stage T_{at} is kept high so that the value of P_{S} will be about one and hence most moves will pass the Metropolis Sampling Test. Initially, as the T_{at} is high, the system can overcome any potential energy barrier and the correct direction is achieved easily. The temperature is decreased gradually which is called the annealing schedule. The T_{at} is a parameter which controls the thermal fluctuation. At higher T_{at}, thermal fluctuation is also high and it helps the system to move out from a local attractive basin towards a deeper energy basin. In later stage of the search, the annealing temperature as well as thermal fluctuation decreases so that the value of P_{S} becomes low. It is essential as in the later stage only, those moves are accepted for which energy decreases. Gradually, when $T_{\text{at}} \rightarrow 0$, the system finds out the desired solution.

2.3 *Quantum chemical calculations*

The SA-based search has generated various low-lying energy structures for $(H_2O)_n\,OH^-$ system (n = 1–6). Now, the geometries of the structures are used as an input for DFT calculations ([with basis set 6-311G++ (d, p) and B3LYP functional]) to obtain frequencies of the IR modes. We have used Gaussian package for quantum chemical calculations. Energies of SA and DFT calculation are different. This is because SA evaluates the energy from empirical potential energy function while DFT evaluates the total energy of the system concerned.

3. Results and discussion

3.1 *Structures and spectroscopy of $(H_2O)_n\,OH^-$ clusters obtained from SA-based search and DFT calculations*

In the literature, vibrational frequencies of water-hydroxide clusters are reported.[50,51,56,93] The IR spectrum of the global minimum clusters are shown in figures 1 and 2. While figure 1 shows IR peaks in the entire frequency range, figure 2 depicts peaks in the range of 3400–4000 cm^{-1}. This is the frequency range where the effects of hydrogen bonding on the stretching modes are expected to be visible. This is done to highlight the high frequency modes and in the larger clusters to prominently display the red-shifted hydrogen bonded peaks with respect to the free O-H stretches. The spectral details are depicted in table 2.

(i) $(H_2O)\,OH^-$

The SA and DFT based structures show close similarity. Both of the structures show one hydrogen atom close to the coordinating OH^- ion. The structures are shown in figure 3a and b, respectively. The H-bond lengths are different in figure 3a and b. This is because the first one is obtained after SA calculation and the second after DFT. The SA calculation uses only a empirical potential and the results are expected to be quantitatively different from the DFT one. The empirical potential in general underestimates the strength of the interaction and hence predicts a larger length as opposed to the more accurate DFT evaluation.

The spectrum of this cluster is shown in figures 1 and 2. In this system, only two peaks of weak intensities are obtained. These are 3816.11 cm^{-1} and 3849.80 cm^{-1} with intensities 18.4159 and 0.8765, respectively. The main contribution to the peak at 3816.11 cm^{-1} occurs due to vibration of the $O(4)$ and $H(5)$ bonds, while the vibration of the $O(1) - H(3)$ bond contributes to the peak at 3849.80 cm^{-1}.

(ii) $(H_2O)_2\,OH^-$

Structures obtained using the SA and DFT are very similar. In both of the cases, there are two O – H$\cdots$O

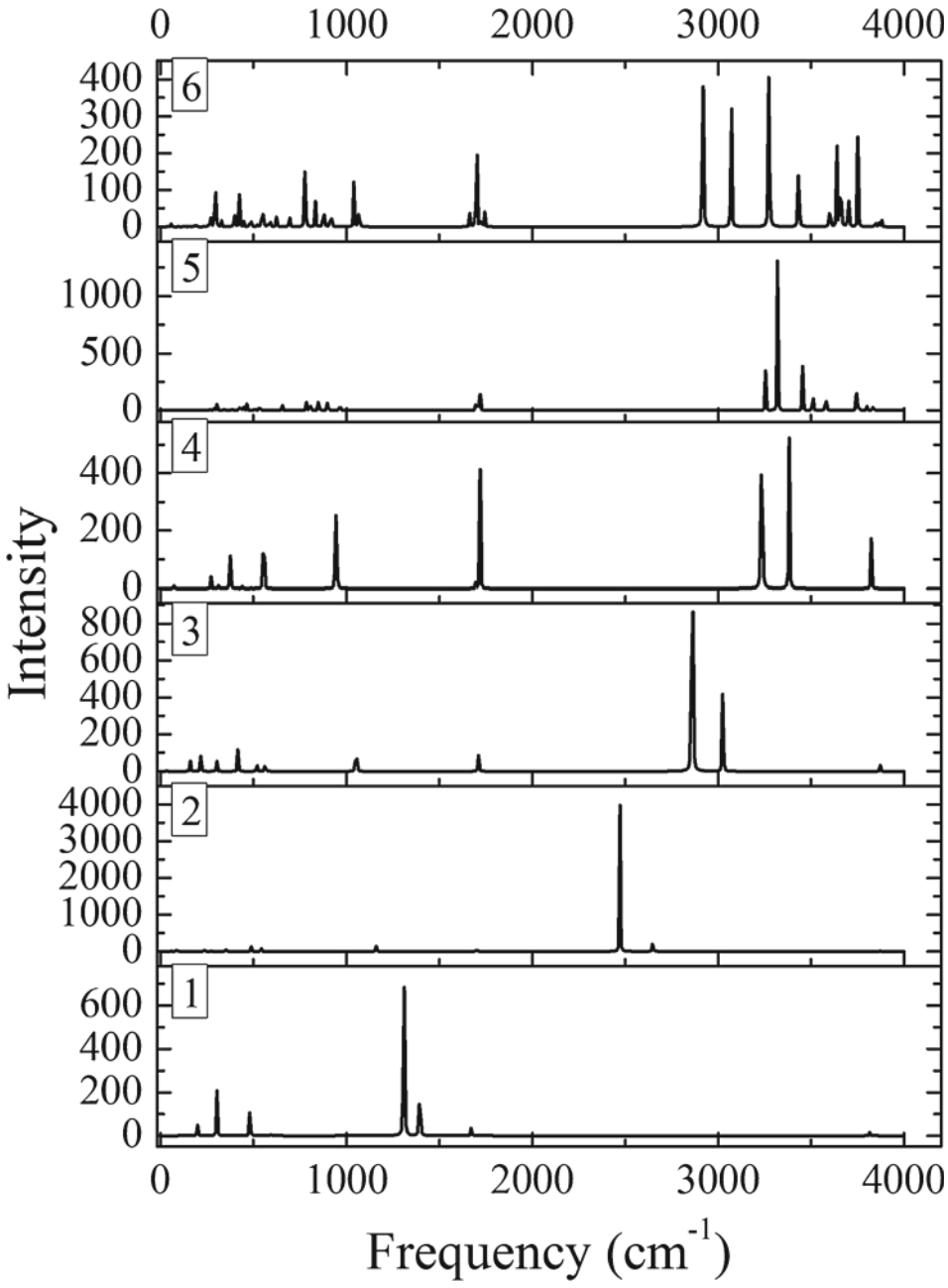

Figure 1. IR spectrum of $(H_2O)_n\,OH^-$ cluster systems.

hydrogen bonds of equal strength and proximity with the central OH^- ion. The other two hydrogen atoms are away from each other in order to minimize the Coulombic interaction between them. The structures are shown in figure 4a and b, respectively. The local structure from SA is shown in figure 4c and it shows that the two $O - H\cdots O$ interactions are of almost equal strength and equal proximity. It is seen from the structures that the two H-bonds present in each have certain noticeable differences. Specifically in figure 4c the two H-bonds are unequal. This is because, figure 4c is a local structure and has some degree of asymmetry compared to the global which is totally symmetric. Generally, in this type of cluster systems the relatively symmetric structure seems to be lower in energy.

The peak at 3842.70 cm^{-1} with relative intensities of 3.5178 occurs due to the vibration of $O(7) - H(8)$ mode. There are two peaks at 3870.03 cm^{-1} and 3870.21 cm^{-1} and their intensities are 3.9091 and 4.3991, respectively. Both of the peaks occur due to $O(1) - H(2)$ bond vibration coupled with $O(4) - H(5)$ bond vibration.

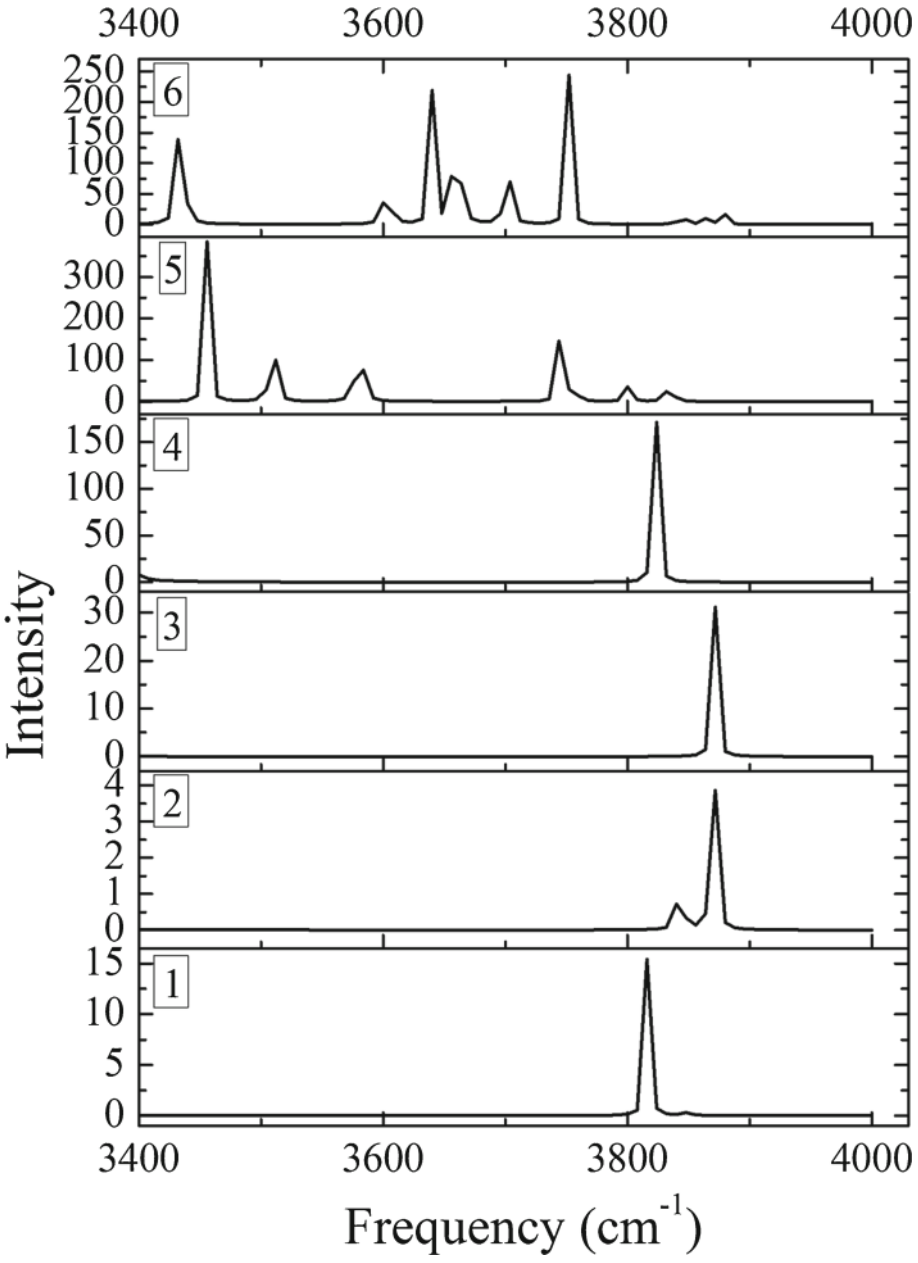

Figure 2. IR spectrum from 3400 to 4000 cm^{-1} of $(H_2O)_n\ OH^-$ cluster systems.

(iii) $(H_2O)_3\ OH^-$

Structures with SA and DFT based method are shown in figure 5a and b, respectively. The SA-based structure similar to a triangular structure while the DFT-based structure looks similar to a tetrahedral one. In both of the cases, there are three O – H···O hydrogen bond interactions of equal strength and equal length. The higher energy structure (local) obtained from SA is shown in figure 5c. The structure is similar to the lower energy structure obtained from SA with slight difference in the three O – H···O interaction lengths.

The IR spectrum of the cluster is shown in figures 1 and 2. For this system we have five vibration frequencies which give rise to five peaks out of which the peak at 3023.40 cm^{-1} has high intensity of 754.9940 and it occur due to $O(1) - H(2)$, $O(4) - H(5)$ and $O(7) - H(8)$ vibration. The peak at 3851.99 cm^{-1} with intensity 0.0025 and originates from $O(10) - H(11)$ vibrational mode. The peak at 3870.89 cm^{-1} with intensity of 11.2489 occur due to $O(1) - H(3)$ and $O(7) - H(9)$ vibrational modes. The peaks at 3871.04 cm^{-1} with 11.5559 intensity and at 3871.51 cm^{-1} with intensity of 13.4634 occur due to bond vibrations involving $O(1) - H(3)$, $O(4) - H(6)$ and $O(7) - H(9)$ simultaneously.

Table 2. Infrared spectroscopic modes of $(H_2O)_n\,OH^-$ clusters.

	Spectral data of $(H_2O)_n\,OH^-$ clusters (O-H) stretching frequencies (cm^{-1})		
Species	DFT calculated (harmonic)	DFT calculated (anharmonic)	Experimental[4–12]
$(H_2O)\,OH^-$	1669, 2144, 3816, 3849	1491, 2029,3656, 3866, 3877	055, 3380, 3653
$(H_2O)_2\,OH^-$	2647, 3842, 3870	2745, 3553, 3858, 3882	2700, 3660, 3694
$(H_2O)_3\,OH^-$	2859, 3023, 3851, 3870, 3871	2609, 2631, 2674, 3682, 3872, 3874	2600, 3695
$(H_2O)_4\,OH^-$	3218, 3233, 3381, 3820, 3823, 3826, 3856	2843, 2875, 2964, 2968, 3434, 3497, 3502,3571, 3620, 3633, 3654, 3683	2900, 3447, 3489, 3615, 3675
$(H_2O)_5\,OH^-$	3253, 3318, 3454, 3508, 3579, 3744, 3754, 3801, 3830, 3835, 3848	3096, 3298, 3357, 3456, 3491, 3523, 3541, 3569, 3605, 3629, 3654, 3698, 3853	3446, 3532, 3572, 3621, 3648, 3700
$(H_2O)_6\,OH^-$	3068, 3272, 3433, 3602, 3639, 3659, 3700, 3751, 3844, 3866, 3867, 3878	2975, 3167, 3400, 3420, 3430, 3472, 3546, 3642, 3869, 3875, 3876	

(iv) $(H_2O)_4\,OH^-$

For this cluster system, the structure with SA and DFT based methods are shown in figure 6a and b, respectively. Both the structures are present on the same line with minor difference in angular disposition and the DFT-based structure is more symmetric than the other one. In both the structures $O - H\cdots O$ bond interaction with the central OH^- ion is present. The local minimum structure with less symmetric and lesser number of $O - H\cdots O$ bonds with central OH^- ion is shown in figure 6c.

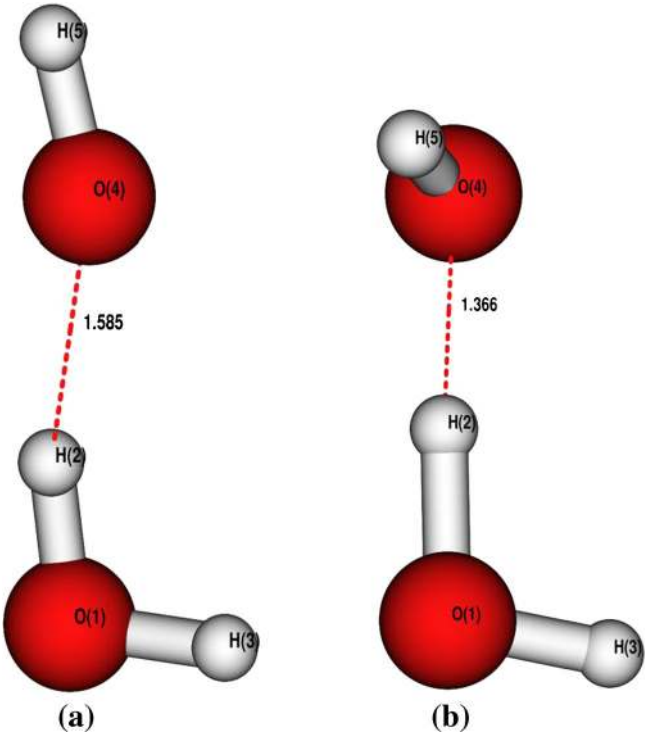

Figure 3. **(a)** Global structure (SA) of $(H_2O)\,OH^-$. **(b)** Global structure (DFT) of $(H_2O)\,OH^-$.

In this system, there are eight peaks in the spectrum range of 3000–4000 cm^{-1}. Two peaks with intensities 1165.5844 and 1165.6159 are at the same position of 3233.79 cm^{-1}. Both of them are highly intense

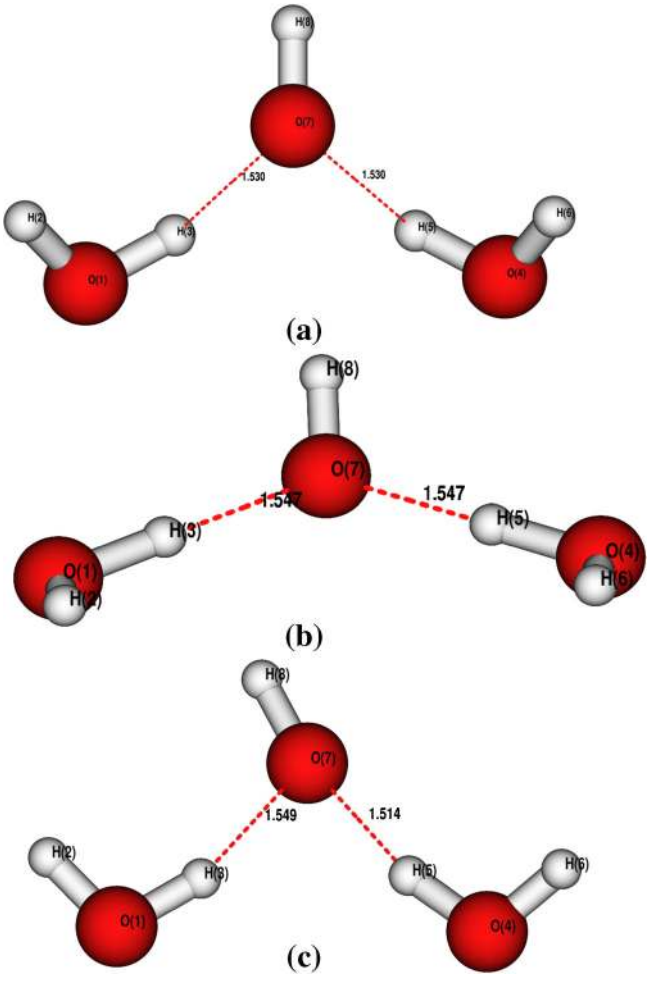

Figure 4. **(a)** Global structure (SA) of $(H_2O)_2\,OH^-$. **(b)** Global structure (DFT) of $(H_2O)_2\,OH^-$. **(c)** Local structure (SA) of $(H_2O)_2\,OH^-$.

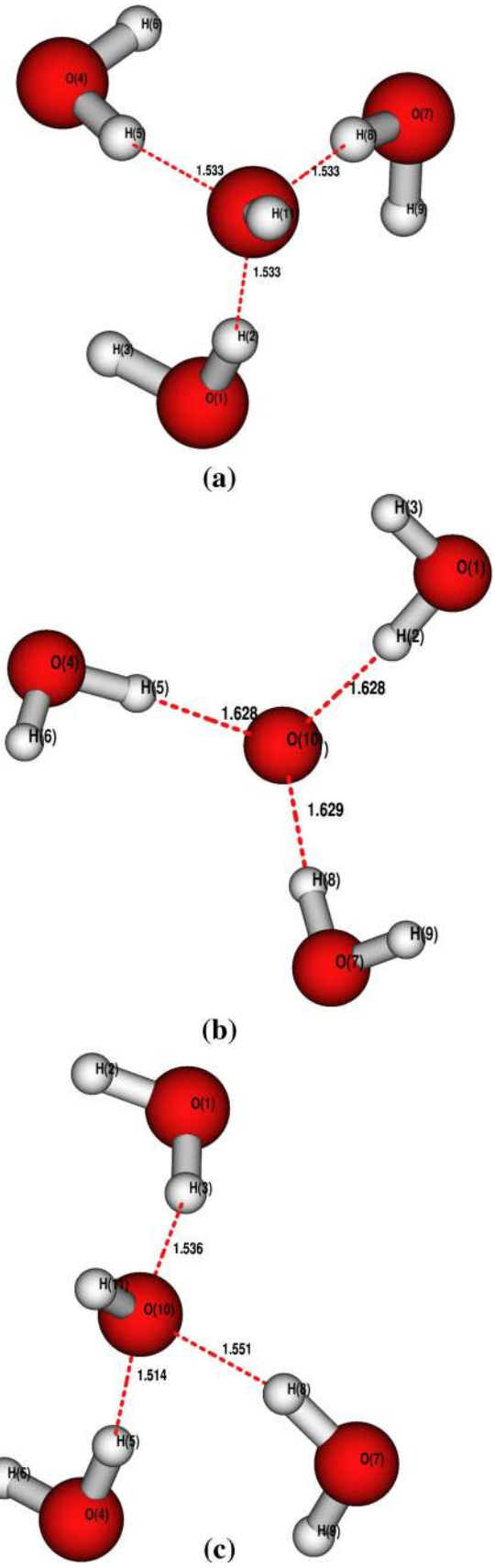

Figure 5. **(a)** Global structure (SA) of $(H_2O)_3\,OH^-$. **(b)** Global structure (DFT) of $(H_2O)_3\,OH^-$. **(c)** Local structure (SA) of $(H_2O)_3\,OH^-$.

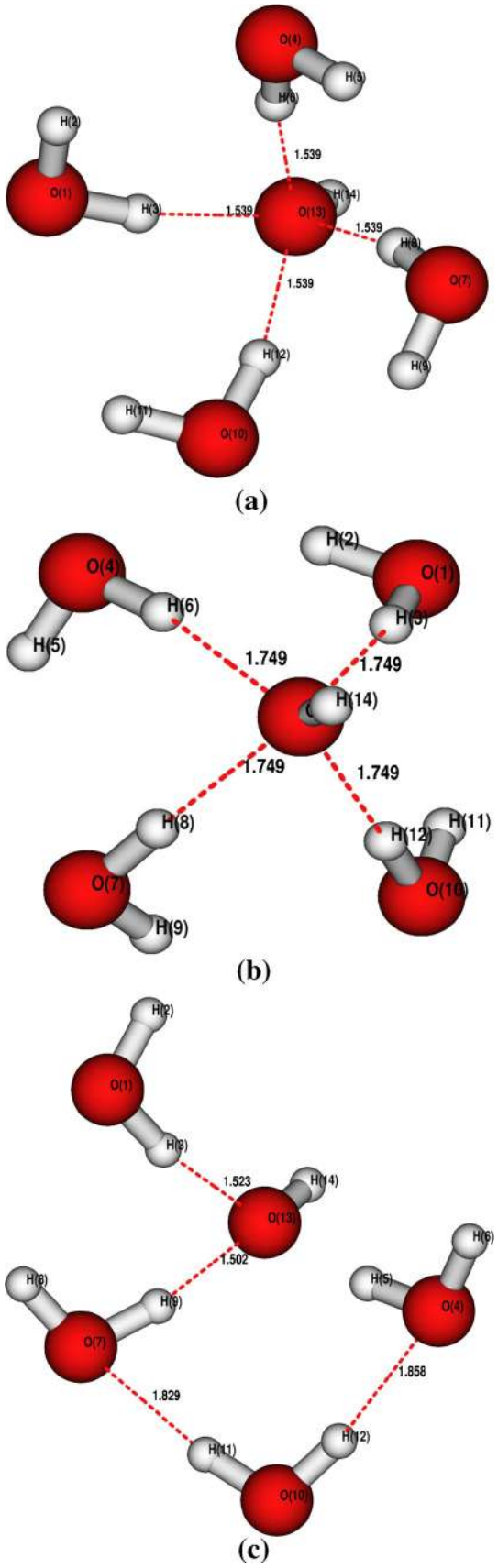

Figure 6. **(a)** Global structure (SA) of $(H_2O)_4\,OH^-$. **(b)** Global structure (DFT) of $(H_2O)_4\,OH^-$. **(c)** Local structure (SA) of $(H_2O)_4\,OH^-$.

in the spectrum and arise due to strong contribution of $O(7) - H(8)$ and $O(1) - H(3)$ vibrational modes with weak contribution of $O(4) - H(6)$ and $O(10) - H(12)$ vibrational modes. The peak at 3381.26 cm^{-1} with strong intensity of 1048.8439 also originates from the above bond vibrations. The peaks at 3820.74 cm^{-1} (67.2507 peak intensity), 3823.80 cm^{-1} (79.3363 peak intensity), 3823.80 cm^{-1} (79.3374 peak intensity) and 3826.61 cm^{-1} (0.0002 peak intensity) occur due to vibrations of $O(1) - H(2)$, $O(4) - H(5)$, $O(7) - H(9)$ and $O(10) - H(11)$ bonds. The peak at 3868.69 cm^{-1} (0.0107 peak intensity) occurs due to $O(13) - H(14)$ vibrational mode. The spectrum of the above system is shown in figures 1 and 2.

(v) $(H_2O)_5\,OH^-$

The SA and DFT based structures for this system are shown in figure 7a and b, respectively. The structures are broadly similar with all the five water molecules having close $O - H\cdots O$ bond interactions with central OH^- ion. However angular dispositions of the non-coordinating hydrogen atoms are slightly different in these two structures. The structure related to local energy is shown in figure 7c. Here, the number of hydrogen-bonded interactions with the central OH^- ion is less than that of global structure.

The IR spectrum corresponding to this system is shown in figures 1 and 2. A total number of 11 peaks are observed in the spectrum. The most intense peak is observed at 3318.59 cm^{-1} (1306.5764 peak intensity) which is due to equally strong contribution of $O(1)-H(2)$ and $O(13)-H(14)$ vibrational modes with weak contribution of $O(4)-H(6)$, $O(7)-H(9)$ and $O(10)-H(12)$ vibrational modes. The peak at 3253.79 cm^{-1} (424.9876 peak intensity) occur mainly due to $O(1)-H(2)$ and $O(13)-H(14)$ vibrations. The peak at 3454.58 cm^{-1} (403.4347 peak intensity) occur due to $O(4)-H(6)$ and $O(7)-H(9)$, at 3508.46 cm^{-1} (391.9892 peak intensity) due to $O(4)-H(6)$, $O(7)-H(9)$ and $O(10)-H(12)$ and at 3579.67 cm^{-1} (486.2181 peak intensity) because of $O(10)-H(12)$ interaction with moderate contribution of $O(4)-H(6)$ and $O(7)-H(9)$ interactions. The other two intense peaks occur at 3744.34 cm^{-1} (190.3778 peak intensity) and at 3754.82 cm^{-1} (130.4440 peak intensity). Both these peaks occur due to $O(7)-H(8)$ and $O(10)-H(11)$ bond interactions.

(vi) $(H_2O)_6\,OH^-$

The two structures obtained from SA and DFT based calculations are shown in figure 8a and b, respectively. Here, we can again see that both the structures

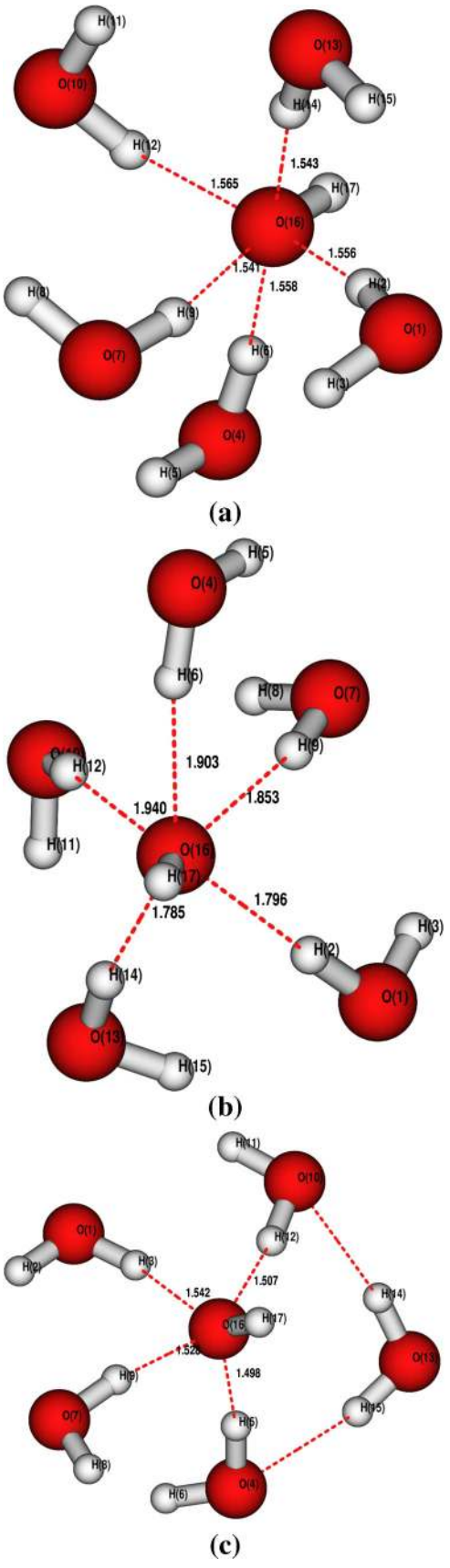

Figure 7. **(a)** Global structure (SA) of $(H_2O)_5\,OH^-$. **(b)** Global structure (DFT) of $(H_2O)_5\,OH^-$. **(c)** Local structure (SA) of $(H_2O)_5\,OH^-$.

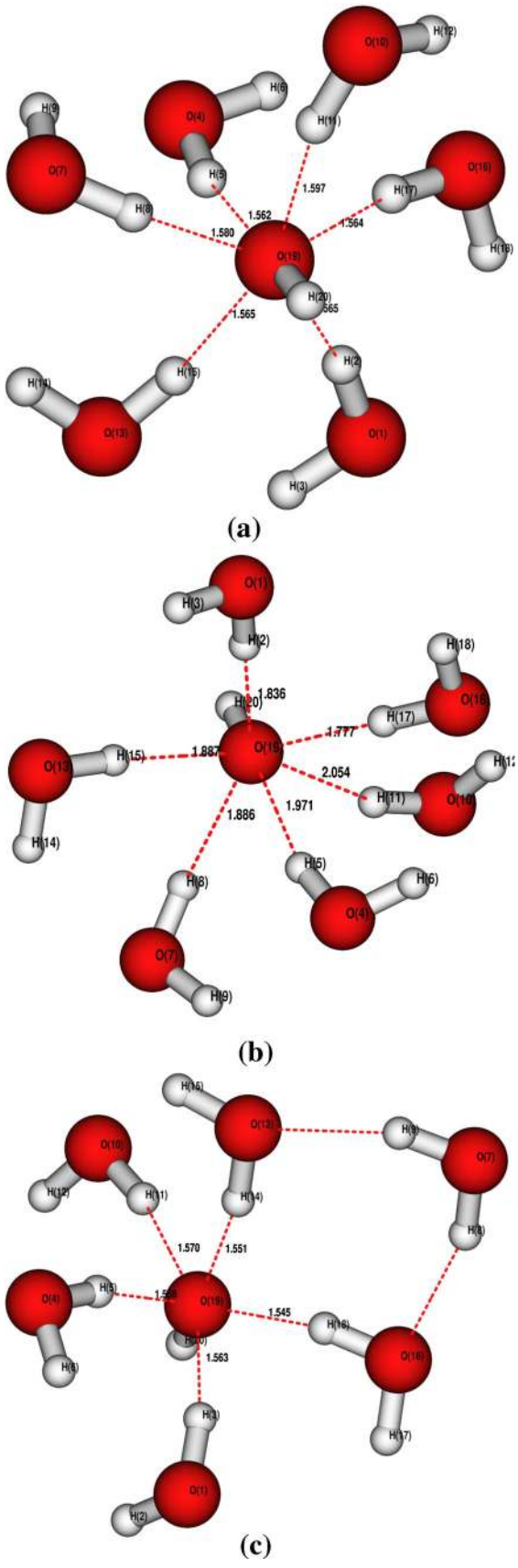

Figure 8. **(a)** Global structure (SA) of $(H_2O)_6\,OH^-$. **(b)** Global structure (DFT) of $(H_2O)_6\,OH^-$. **(c)** Local structure (SA) of $(H_2O)_6\,OH^-$.

are essentially similar with minor difference in spatial orientation. In both the structures, all the six water molecules are close to the coordinating OH^- ion and are able to form $O-H\cdots O$ hydrogen bonded interactions. Figure 8c shows the local energy structure where five water molecules are close proximity to the central OH^- ion.

The IR spectrum of the cluster obtained from the DFT calculation is shown in figures 1 and 2. The system generates 12 peaks between 3000 and 4000 cm^{-1}. The peak at 3272.84 cm^{-1} (1352.0379 peak intensity) is the most intense peak and it originates from $O(1)-H(2)$ vibrational mode with moderate contribution from $O(7)-H(8)$, $O(13)-H(15)$ and $O(16)-H(17)$ modes. The second most intense peak is at 3068.52 cm^{-1} (690.2588 peak intensity) and is due to $O(1)-H(2)$ and $O(16)-H(17)$ interactions. The third one occurs, at 3659.15 cm^{-1} (572.3403 peak intensity) and occurs, due to $O(4)-H(5)$, $O(4)-H(6)$ interactions. The vibrational mode $O(10)-H(11)$ and $O(10)-H(12)$ contributes to the peak at 3639.64 cm^{-1} (227.5687 peak intensity) and at 3751.28 cm^{-1} (249.0348 peak intensity). The peak at 3433.27 cm^{-1} (496.8191 peak intensity) occurs due to $O(7)-H(8)$ vibrational mode; at 3602.55 cm^{-1} (205.1738 peak intensity) occurs due to $O(4)-H(5)$ and $O(4)-H(6)$ vibrational modes. The peak at 3701.00 cm^{-1} is also moderately intense (245.6067 peak intensity) and it originates from $O(7)-H(8)$ and $O(7)-H(9)$ vibrational modes coupled with $O(4)-H(5)$ and $O(4)-H(6)$ vibrational modes. Another intense peak is observed at 3751.28 cm^{-1} (249.0348 peak intensity), which is a contribution of $O(10)-H(11)$ vibrational mode coupled with $O(10)-H(12)$ vibrational mode.

The global minimum of all the cluster systems is that for which all the OH bonds in H_2O coordinates are close to the central OH^- ion and has been observed in earlier studies.[50] The local minima from $n = 4$ onwards have structures with fewer H_2O molecules coordinating directly with the central OH^- ion and engaging in H-bonds with other H_2O molecules at some distance away from the central OH^- ion.

The energies of SA and DFT calculation are different. This is because SA evaluates the energy from empirical potential energy function while DFT evaluates the total energy of the system concerned. The energy values are given in table 3.

It is worthwhile to discuss the trends in the hydrogen bond lengths as well as the strength of the H-bond as one changes the size of $(H_2O)_n\,OH^-$ clusters. As evident from the structures of the clusters depicted in the figures, the H-bond length gradually increases from around 1.37 A for $n = 1$ to a high value of 2.054 for

Table 3. Energy values obtained from SA and DFT calculations.

	Energy values from SA and DFT calculation			
Species	Global SA (kcal/mol)	Global DFT (kcal/mol)	Local SA (kcal/mol)	Local DFT (kcal/mol)
$(H_2O)\ OH^-$	−27.2465	−152.3328		
$(H_2O)_2\ OH^-$	−73.7531	−228.8282	−71.8180	−228.8053
$(H_2O)_3\ OH^-$	−113.1241	−305.3183	−108.7989	−305.2954
$(H_2O)_4\ OH^-$	−146.7705	−381.8021	−132.3167	−381.7670
$(H_2O)_5\ OH^-$	−175.4105	−458.2778	−165.5462	−458.2400
$(H_2O)_6\ OH^-$	−195.3597	−534.7640	−184.6904	−534.6995

some of the H-bonds in $n = 6$ cluster. This result is seen from following the structures evaluated after the DFT stage. This is an expected trend since the single hydroxide ion engages in a larger number of interactions with more water molecules with increasing size of the cluster. Hence, we expect a single H-bond formed by interacting with the oxygen of the hydroxide ion to be larger in length compare to the case in which there is only a single H-bond formed as is the case for $n = 1$ cluster. The structure evaluated after the SA stage also shows an increase in the H-bond length, though its effect is not as pronounced as the DFT calculation. This is again expected because the SA calculation employs only an empirical potential and its quantitative accuracy has to be less than a rigorous quantum chemical calculation done at some level of theory. The DFT calculation can also give us the magnitude of H-bond interaction energy for each of the cluster systems. This is now depicted in table 4. The total H-bonded energy shows a gradual increase, as expected, since the number of H-bonds formed increase with increase in cluster size.

In continuation with the ongoing discussion, it is worthwhile to note certain trends in the bond parameters (H-bond distances) after SA calculation and the DFT level. The SA evaluated structures show a gradual increase in H-bonded distances while in DFT, the increase is appreciable. This is a more acceptable trend because the DFT calculation are expected to be more accurate than the SA, which uses the TIP3P model potential for water. The TIP3P model does not incorporate polarization corrections and assumes the charges to be localized on the hydrogen and oxygen centres.[123] So in principle, this is a point charge model and does not allow any room for charge delocalization, which is the feature of any quantum chemical system. This is the main reason for the discrepancy in the values at the two levels of theory. Our motivation for using SA was to quickly generate good quality pre-optimized structures which though not perfectly accurate in terms of individual bond parameters, are perfect from the point of view of symmetry. After DFT calculation, we can observe that the symmetry of the structure does not change much but the individual bond parameters are obviously updated. Another noticeable feature is the difference in magnitudes of the H-bonds in the local minima as compared to the global one, at least in the smaller size clusters. This can be explained in the sense that the local structures are relatively asymmetric compared to the global one and are bound to show this trend.

Table 4. Hydrogen bond energies obtained from DFT calculations on $(H_2O)_n\ OH^-$ cluster systems.

Species	Hydrogen bond energy (a.u)
$(H_2O)\ OH^-$	−0.046838
$(H_2O)_2\ OH^-$	−0.083663
$(H_2O)_3\ OH^-$	−0.115287
$(H_2O)_4\ OH^-$	−0.140534
$(H_2O)_5\ OH^-$	−0.157687
$(H_2O)_6\ OH^-$	−0.170226

We have also calculated the frequencies of these studied cluster systems incorporating anharmonic corrections. This was done with a view to see if coupling of the standard harmonic modes due to the anharmonic perturbation plays a significant role or not. Generally, it is observed that in such systems where the central encapsulated entity is an ion, couple between modes should become prominent and the frequencies evaluated at this level of theory should be closer to the experimentally reported values. In fact, this is what we observe in most cluster sizes, if we refer to the values presented in table 2. Especially, if we look at clusters $(H_2O)_2\ OH^-$, $(H_2O)_3\ OH^-$, $(H_2O)_4\ OH^-$, the position of highly intense ionic H-bonded is much better evaluated with anharmonic correction and agreement with experiment is close. Specifically, for $(H_2O)_2\ OH^-$, the experimental peak[4–12] is at 2700 cm^{-1} while the anharmonic theory predicts a value of 2745 cm^{-1}. Harmonic approximation result shows greater deviation with a calculated value of 2647 cm^{-1}. For $(H_2O)_3\ OH^-$ and $(H_2O)_4\ OH^-$, the agreements are excellent where the theoretical predicted frequencies is within 15 wavenumber of the experimentally reported

one. For $(H_2O)_5\,OH^-$, again, the theoretically reported value is within 10 wavenumber So, we can certainly conclude that coupling of modes induced by anharmonicity plays a significant role in this systems.

The evaluated theoretical frequencies can also be compared with reported theoretical ones. However, the correspondence might not be of a high degree as the values change significantly with change in the level of theory.[50] Our effort with B3LYP functional and with anharmonicity corrections predicts values which do not differ significantly from the experiment.

The NPA (Natural Population Analysis) charges for the global minimum structures $(H_2O)_n\,OH^-$ $n = 1$–6 have been determined to see if the charges evaluated can throw some light on trends in the VDE (Vertical Detachment Energy) of the cluster systems. Table 5 lists these parameters. Charges on the oxygen and hydrogen atoms of the hydroxyl group and the charges on the hydrogen atoms bound to the oxygen of the OH^- by hydrogen bonding are listed in columns 2–4. The fifth colum lists the VDEs for the various cluster sizes. If we look at the individual NPA charges on the atoms, the difference between them are marginal though there seems to be a slight gradual increase in the positive charge on the hydrogen of the hydroxyl ion as the size of the cluster increases. However, the trend is not so regular for oxygen atom of hydroxyl ion. But, it must also be noted that the difference between magnitude of charges on various atoms as the cluster size increases, is only nominal. So, we can come to a reasonably correct conclusion that the strengths of various hydrogen bonds present in the different cluster systems do no differ much. However, the number of hydrogen bonds present increases rapidly with the increase in cluster size. For this mononegative cluster systems, the predominant portion of the excess negative charge is expected to be located on the oxygen atom of the hydroxyl group. As the size of the cluster increases, the oxygen atom of the hydroxyls gets much strongly bound to the surrounding water molecules on account of the obvious increase in the number of hydrogen-bonded interactions. So, if one calculates the VDE, it is expected that it will be the highest for $(H_2O)_6\,OH^-$ and least for $(H_2O)\,OH^-$ with a gradual increase with increase in size of the clusters. This is reflected in calculation of VDE (table 5) and plot of the variation of VDE with size (figure 9).

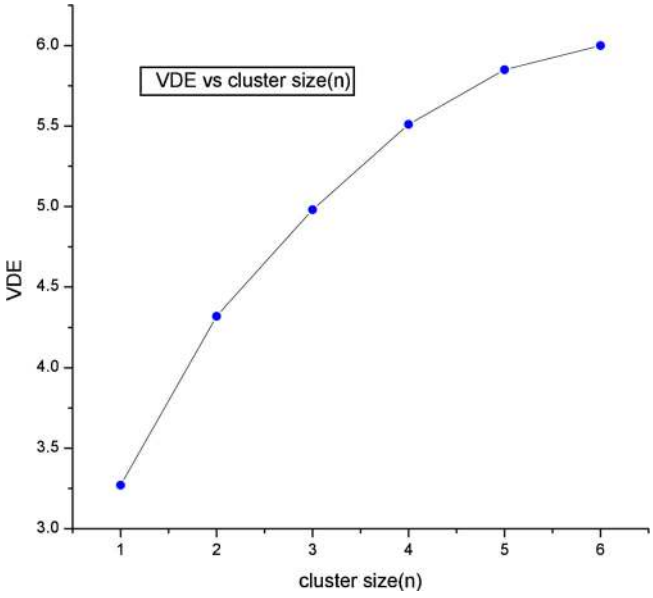

Figure 9. Plot of VDE vs cluster size (n) of $(H_2O)_n\,OH^-$ systems.

3.2 *Atoms in molecule (AIM)-based study of topological analysis*

A study on cluster systems involving H-bonding can be efficiently conducted by using the AIM method of Bader[119] and the strategy suggested by Koch and

Table 5. NPA charge and VDE calculation of $(H_2O)_n\,OH^-$ clusters.

NPA charge and VDE calculation of $(H_2O)_n\,OH^-$ clusters				
Species	O atom of hydroxyl ion	H atom of hydroxyl ion	H atoms of surrounding water molecules	VDE in eV
$(H_2O)\,OH^-$	−1.206	0.393	H(2) = 0.483	3.27
$(H_2O)_2\,OH^-$	−1.220	0.415	H(3) = 0.506, H(5) = 0.506	4.32
$(H_2O)_3\,OH^-$	−1.213	0.430	H(2) = 0.505, H(5) = 0.504, H(8) = 0.505	4.98
$(H_2O)_4\,OH^-$	−1.254	0.438	H(3) = 0.499, H(6) = 0.500, H(8) = 0.499, H(12) = 0.500	5.51
$(H_2O)_5\,OH^-$	−1.278	0.443	H(2) = 0.496, H(6) = 0.489, H(9) = 0.494, H(12) = 0.498, H(14) = 0.494	5.85
$(H_2O)_6\,OH^-$	−1.235	0.449	H(2) = 0.496, H(5) = 0.486, H(8) = 0.496, H(11) = 0.484, H(15) = 0.507, H(17) = 0.509	6.00

Numbers in the bracket correspond to the H atoms which are attached to the central OH^- ion.

Popelier.[120] This method has been extensively used in a number of impressive application.[121–125] To describe an interaction as a hydrogen bonded one, certain criteria should be satisfied based on the AIM technique.

1. The existence of a bond critical point (BCP) between the corresponding hydrogen atom and the acceptor atom engaged in the interaction.
2. Magnitude of the electron density parameter $\rho(r)$ (which is the main criterion to check whether a H-bond has been created or not) evaluated at the BCP must be within a specified range [0.002–0.004 a.u]
3. Moreover, the Laplacian of electron density at the BCP $\left(\nabla^2\rho_c\right)$ must be +ve and should be within the range of 0.02–0.15 a.u.
4. Bonded radius of the hydrogen atom and the corresponding acceptor atom must individually be less than the corresponding van der Waals radii while in the non-bonded state, further, an estimate of H-bond energy can be made as this is connected to the local potential energy density at the hydrogen bond critical point along with the atomic volume element using the following equation.

$$E_{\mathrm{Hb}} = -\frac{a_0^3}{2}V_{\mathrm{ep}}. \tag{5}$$

We have pictorially depicted the AIM-evaluated structures connecting the electron density $\rho(r)$ along with the location of critical points in figure 10a–f. Moreover, we report in tabular form, the magnitudes of all the necessary parameters evaluated using the AIM study and

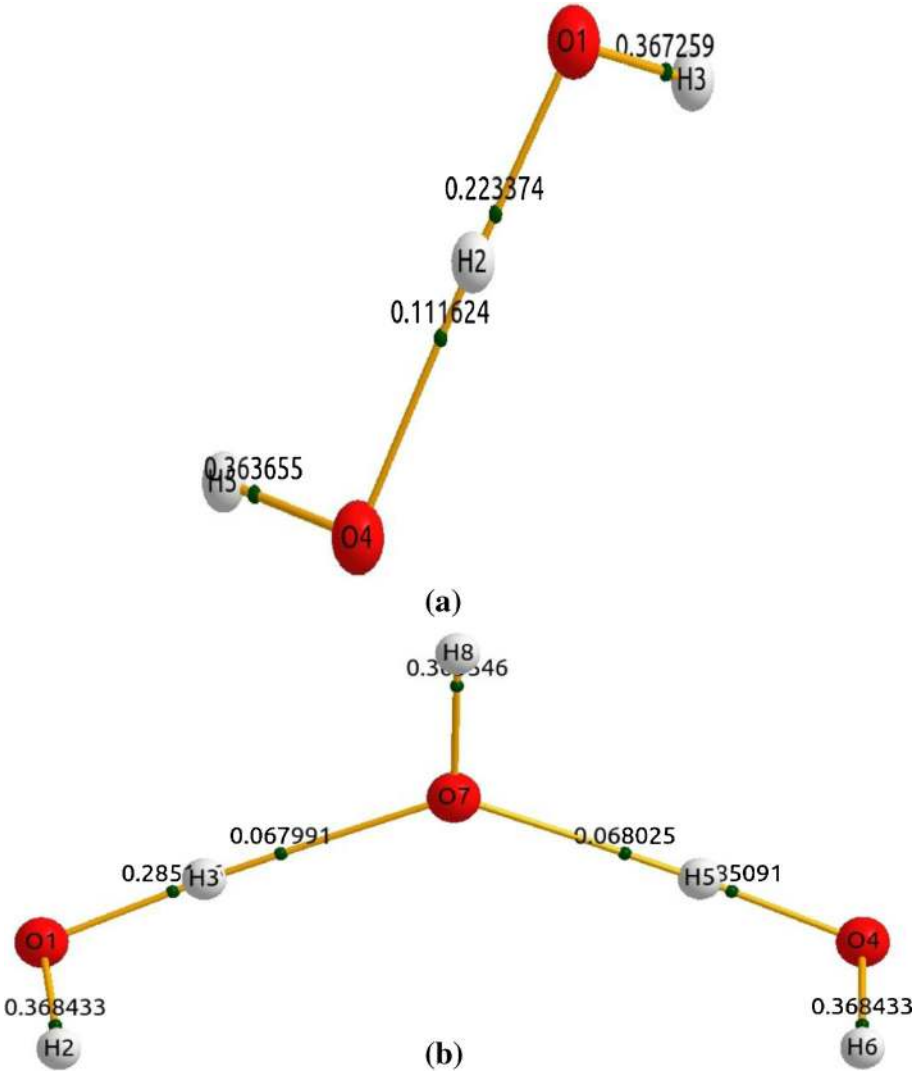

Figure 10. **(a)** Global structure (AIM) of $(H_2O)\,OH^-$. **(b)** Global structure (AIM) of $(H_2O)_2\,OH^-$. **(c)** Global structure (AIM) of $(H_2O)_3\,OH^-$. **(d)** Global structure (AIM) of $(H_2O)_4\,OH^-$. **(e)** Global structure (AIM) of $(H_2O)_5\,OH^-$. **(f)** Global structure (AIM) of $(H_2O)_6\,OH^-$.

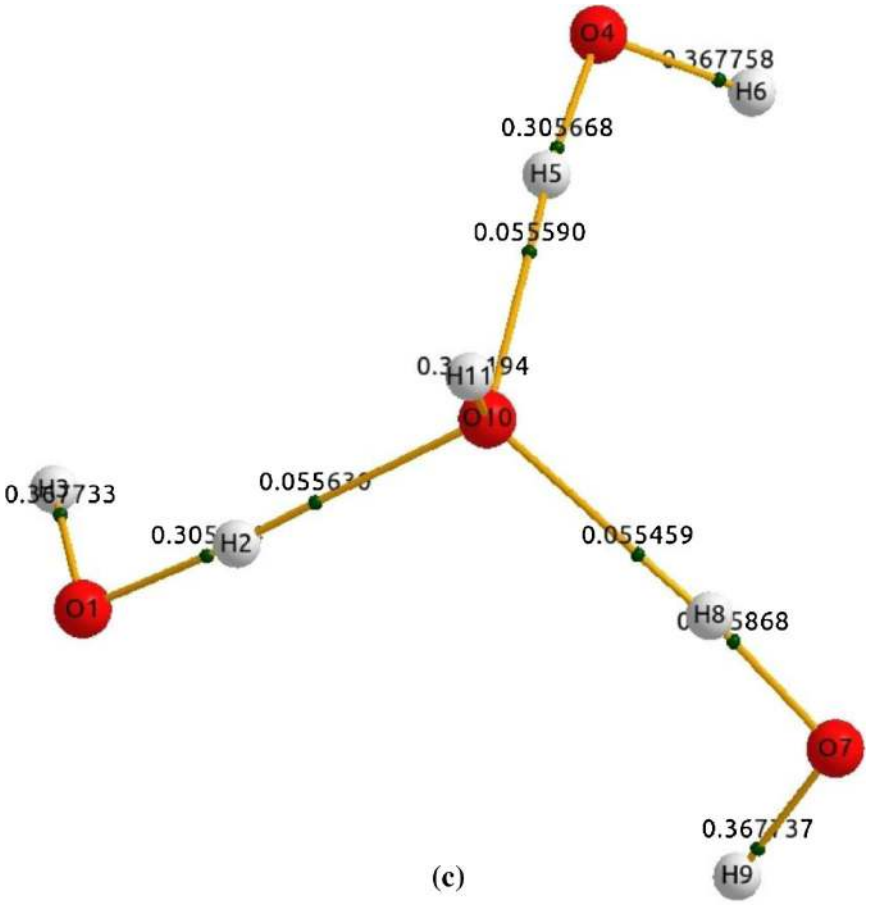

(c)

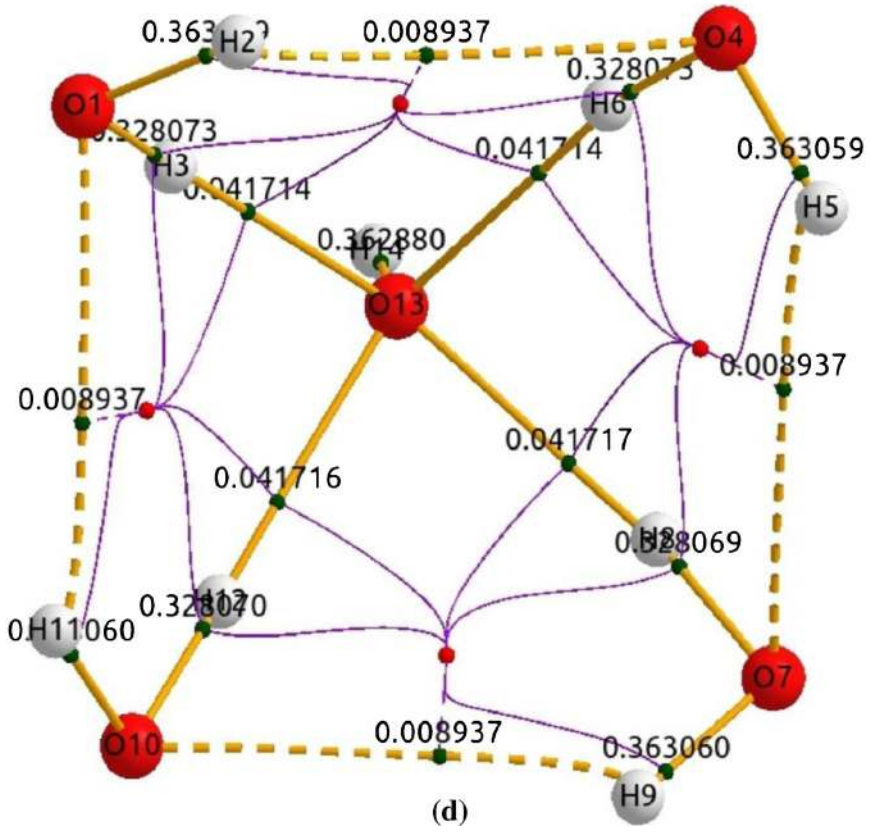

(d)

Figure 10. (*cont.*)

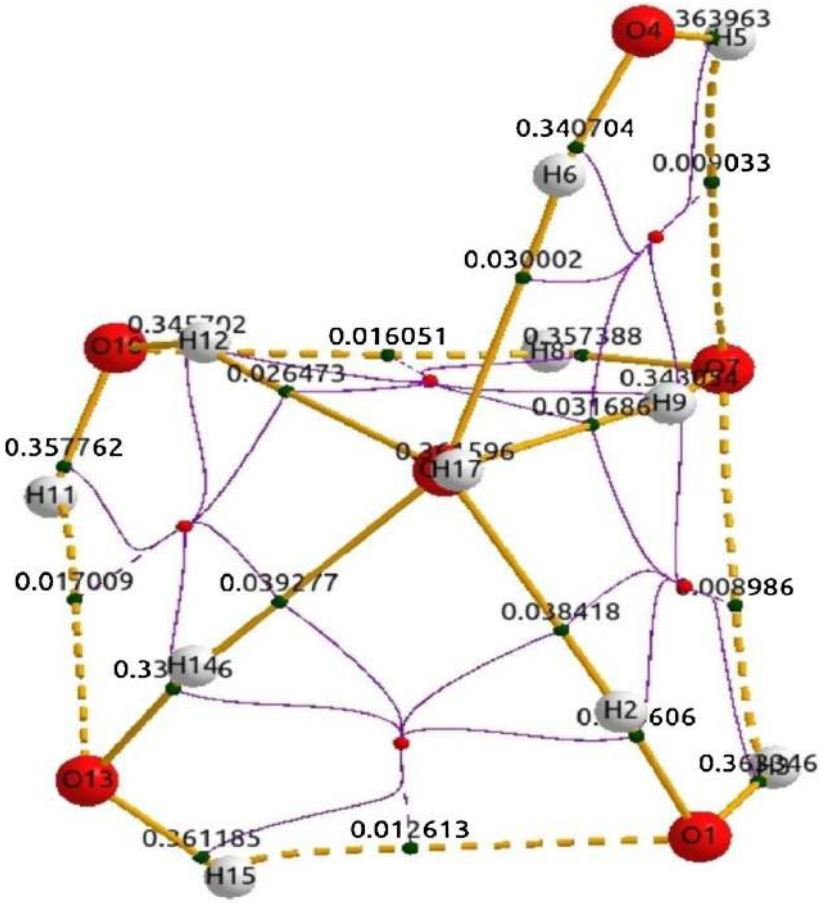

Figure 10. (*cont.*)

Table 6. Details of results obtained from AIM calculations on the $(H_2O)_n\ OH^-$ clusters.

Species	Name	Atoms	Rho	DelSqRho	Ellipticity	H	V	G	Energy = V/2
$(H_2O)\ OH^-$	BCP 3	H2–O4	0.111624	+0.079537	0.036085	−0.055566	−0.131016	+0.075450	−0.065508
$(H_2O)_2\ OH^-$	BCP 2	H3–O7	0.067991	+0.145149	0.045084	−0.017092	−0.070472	+0.053380	−0.0352360
	BCP 4	H5–O7	0.068025	+0.145167	0.045047	−0.017113	−0.070519	+0.053405	−0.0352595
$(H_2O)_3\ OH^-$	BCP 7	H2–O10	0.055630	+0.141128	0.046984	−0.009535	−0.054351	+0.044817	−0.0271755
	BCP 8	H5–O10	0.055590	+0.141139	0.046942	−0.009511	−0.054306	+0.044795	−0.0271530
	BCP 9	H8–O10	0.055459	+0.140943	0.046959	−0.009444	−0.054123	+0.044679	−0.0270615
$(H_2O)_4\ OH^-$	BCP 13	H3–O13	0.041714	+0.125077	0.047332	−0.002966	−0.037202	+0.034235	−0.0186010
	BCP 14	H6–O13	0.041714	+0.125077	0.047330	−0.002966	−0.037202	+0.034236	−0.0186010
	BCP 15	H8–O13	0.041717	+0.125082	0.047330	−0.002967	−0.037205	+0.034238	−0.0186025
	BCP 16	H12–O13	0.041716	+0.125081	0.047332	−0.002967	−0.037205	+0.034237	−0.0186025
$(H_2O)_5\ OH^-$	BCP 3	H9–O16	0.031686	+0.108703	0.066850	+0.000447	−0.026282	+0.026729	−0.0131410
	BCP 5	H6–O16	0.030002	+0.091253	0.046198	+0.000031	−0.022751	+0.022782	−0.0113755
	BCP 11	H12–O16	0.026473	+0.092155	0.026998	+0.001193	−0.020653	+0.021846	−0.0103265
	BCP 19	H2–O16	0.038418	+0.112085	0.064669	−0.002150	−0.032322	+0.030172	−0.0161610
	BCP 20	H14–O16	0.039277	+0.115752	0.042140	−0.002358	−0.033654	+0.031296	−0.0168270
$(H_2O)_6\ OH^-$	BCP 1	H2–O19	0.034851	+0.104422	0.054323	−0.001006	−0.028117	+0.027111	−0.0140585
	BCP 4	H5–O19	0.021489	+0.087124	0.012214	+0.002604	−0.016574	+0.019177	−0.0082870
	BCP 8	H15–O19	0.031090	+0.096038	0.055404	−0.000066	−0.024140	+0.024075	−0.0120700
	BCP 9	H8–O19	0.031229	+0.096304	0.074627	−0.000160	−0.024395	+0.024236	−0.0121975
	BCP 12	H17–O19	0.039534	+0.116798	0.046218	−0.002334	−0.033868	+0.031534	−0.016934
	BCP 13	H11–O19	0.022032	+0.067680	0.023325	+0.000874	−0.015172	+0.016046	−0.007586

this is represented in table 6. The table along with other necessary values contains the electron density as well as the H-bond energy for each and every H-bond existing in all the cluster systems, that is $(H_2O)_n\ OH^-$ where $n = 1$–6.

4. Conclusion

This study demonstrates the utility of a strategy based on combined SA and DFT to study structure and spectroscopic aspects of water-hydroxide ion clusters. The simple strategy discussed here can answer many questions related to spectral shits of different size clusters. We wish to extend our strategy to many fascinating systems in future communications.

References

1. Wang Y S, Chang H C, Jiang J C, Lin S H, Lee Y T and Chang H-C 1998 *J. Am. Chem. Soc.* **120** 8777
2. Klots C E and Compton R N 1978 *J. Chem. Phys.* **69** 1644
3. Knapp M, Echt O, Kreisle D and Recknagel E 1986 *J. Chem. Phys.* **85** 636
4. Schulz P A, Mead R D, Jones P L and Lineberger W C 1982 *J. Chem. Phys.* **77** 1153
5. Owrutsky J C, Rosenbaum N H, Tack L M and Saykally R J 1985 *J. Chem. Phys.* **83** 5338
6. Martin J M L 2001 *Spectrochim. Acta. Part A* **57** 875
7. Klots C E and Compton R N 1978 *J. Chem. Phys.* **69** 1644
8. Mautner M 1986 *J. Am. Chem. Soc.* **108** 6189
9. Yang X and Castleman A W 1990 *J. Phys. Chem.* **94** 8500
10. Schindler T, Berg C, Niedner-Schatteburg G and Bondybey V E 1995 *J. Phys. Chem.* **99** 12434
11. Robertson W H, Diken E G, Price E A, Shin J-W and Johnson M A 2003 *Science* **299** 1367
12. Price E A, Robertson W H, Diken E G, Weddle G H and Johnson M A 2002 *Chem. Phys. Lett.* **366** 412
13. Arshadi M and Kebarle P 1970 *J. Phys. Chem.* **74** 1483
14. Mautner M and Speller C V 1986 *J. Phys. Chem.* **90** 6616
15. Payzant J D, Yamdagni R and Kebarle P 1971 *Can. J. Chem.* **49** 3308
16. Fraley P E and Rao K N 1969 *J. Mol. Spectrosc.* **29** 348
17. Buck U and Huisken F 2000 *Chem. Rev. (Washington, D.C.)* **100** 3863
18. Joseph R Roscioli, Eric G Diken, Mark A Johnson, Samantha Horvath and Anne B McCoy 2006 *J. Phys. Chem. A* **110** 4943
19. Jorgensen W L and Madura J D 1983 *J. Am. Chem. Soc.* **105** 1407
20. Jorgensen W L, Chandrasekhar J, Madura J D, Impey R W and Klein M L 1983 *J. Chem. Phys.* **79** 926
21. Jorgensen W L 1981 *J. Am. Chem. Soc.* **103** 335
22. Berendsen H J C, Postma J P M, vanGunsteren W F and Hermans J 1981 *Intermolecular forces* (ed.) Pullman B (Dordrecht: Reidel)
23. Berendsen H J C, Grigeria J R and Straatsma T P 1987 *J. Phys. Chem.* **91** 6269
24. Wales D J and Hodges M P 1998 *Chem. Phys. Lett.* **286** 65
25. Chaudhury P, Saha R and Bhattacharya S P 2001 *Chem. Phys.* **270** 277
26. Horn H W, Swope W C, Pitera J W, Madura J D, Dick T J, Hura G L and Head-Gordon T 2004 *J. Chem. Phys.* **120** 9665
27. Abascal J L F, Sanz E, Fernández R G and Vega C 2005 *J. Chem. Phys.* **122** 234511
28. Abascal J L F and Vega C 2005 *J. Chem. Phys.* **123** 234505
29. Stillinger F H and Rahaman A 1974 *J. Chem. Phys.* **60** 1545
30. Dyer K M, Perkyns J S, Stell G and Pettitt B M 2009 *Mol. Phys.* **107** 423
31. Mahoney M W and Jorgensen W L 2000 *J. Chem. Phys.* **112** 8910
32. Rick S W 2004 *J. Chem. Phys* **120** 6085
33. Pliego J R and Riveros J M 2000 *J. Chem. Phys.* **112** 4045
34. Newton M D and Ehrenson S 1971 *J. Am. Chem. Soc.* **93** 4271
35. Ross B O, Kraemer W P and Diercksen G H F 1976 *Theor. Chim. Acta* **42** 77
36. Szczesniak M M and Scheiner S 1982 *J. Chem. Phys.* **77** 4586
37. Rohlfing C M, Allen L C, Cook C M and Schlegel H B 1983 *J. Chem. Phys.* **78** 2498
38. Sapse M, Osorio L and Snyder G 1984 *Int. J. Quantum Chem.* **26** 223
39. Gao J, Garner D S and Jorgensen W L 1986 *J. Am. Chem. Soc.* **108** 4784
40. Del Bene J E 1988 *J. Phys. Chem.* **92** 2874
41. Bankura A and Chandra A 2011 *Chem. Phys.* **387** 92
42. Bankura A and Chandra A 2012 *Chem. Phys.* **400** 154
43. Pratihar S and Chandra A 2011 *J. Chem. Phys.* **134** 034302
44. Pratihar S and Chandra A 2010 *J. Phys. Chem.* **114** 11869
45. Grimm A R, Bacskay G B and Haymet A D 1995 *J. Mol. Phys.* **86** 369
46. Tunon I, Rinaldi D, Ruiz-Lopez M F and Rivail J L 1995 *J. Phys. Chem.* **99** 3798
47. Xantheas S S 1995 *J. Am. Chem. Soc.* **117** 10373
48. del Valle C P and Novoa J J 1997 *Chem. Phys. Lett.* **269** 401
49. Turki N, Milet A, Rahmouri A, Ouamerali O, Moszynski R, Kochanski E and Wormer P E S 1998 *J. Chem. Phys.* **109** 7157
50. Lee H M, Tarkeshwar P and Kim K S 2004 *J. Chem. Phys.* **121** 4657
51. Wei D, Proynov E I, Milet A and Salahub D R 2000 *J. Phys. Chem. A* **104** 2384
52. Neogi S G and Chaudhury P 2012 *J. Comput. Chem.* **33** 629
53. Masamura M 2002 *J. Chem. Phys.* **117** 5257
54. Masamura M 2001 *Chem. Phys. Lett.* **339** 279
55. Mejias J A and Lago S 2000 *J. Chem. Phys.* **113** 7306
56. Chaudhuri C, Wang Y S, Jiang J C, Lee Y T, Chang H C and Niedner-Schatteburg G 1161 *Mol. Phys.* 99.
57. Becke A D 1988 *Phys. Rev. A* **38** 3098

58. Lee C, Yang W and Parr R G 1988 *Phys. Rev. B* **37** 785
59. Pudzianowski A T 1995 *J. Chem. Phys.* **102** 8029
60. Pudzianowski A T 1996 *J. Phys. Chem.* **100** 4781
61. Tuckerman Mb E, Marx D, Klein M L and Parrinello M 1997 *Science* **275** 817
62. Lee H M, Suh S B, Lee J Y, Tarakeshwar P and Kim K S 2000 *J. Chem. Phys.* **112** 9759
63. Kim J, Majumdar D, Lee H M and Kim K S 1999 *J. Chem. Phys.* **111** 9128
64. Kim J and Kim K S 1998 *J. Chem. Phys.* **109** 5886
65. Kim K S, Mhin B J, Choi U S and Lee K 1992 *J. Chem. Phys.* **97** 6649
66. Kim K S, Dupuis M, Lie G C and Clementi E 1986 *Chem. Phys. Lett.* **131** 451
67. Tsai C J and Jordan K D 1993 *Chem. Phys. Lett.* **213** 181
68. Fowler J E and Schaefer III H F 1995 *J. Am. Chem. Soc.* **117** 446
69. Franken K A, Jalaie M and Dykstra C E 1992 *Chem. Phys. Lett.* **198** 59.
70. Burnham C J, Xantheas S S, Miller M A, Applegate B E and Miller R E 2002 *J. Chem. Phys.* **117** 1109
71. Lee H M, Lee S and Kim K S 2003 *J. Chem. Phys.* **119** 187
72. Lee H M, Suh S B and Kim K S 2003 *J. Chem. Phys.* **118** 9981
73. Lee H M and Kim K S 2002 *J. Chem. Phys.* **117** 706
74. Suh S B, Lee H M, Kim J, Lee J Y and Kim K S 2000 *J. Chem. Phys.* **113** 5273
75. Kim J, Suh S B and Kim K S 1999 *J. Chem. Phys.* **111** 10077
76. Kim J, Lee J Y, Oh K S, Park J M, Lee S and Kim K S 1999 *Phys. Rev. A* **59** R930
77. Novakovskaya Y V and Stepanov N F 2001 *Chem. Phys. Lett.* **344** 619
78. Kulkarni S A, Bartolotti L J and Pathak R K 2000 *J. Chem. Phys.* **113** 2697
79. Tachikawa H, Lund A and Ogasawara M 1993 *Can. J. Chem.* **71** 118
80. Wang F and Jordan K D 2003 *J. Chem. Phys.* **119** 11645
81. Lee S and Lee H M 2003 *Bull. Korean Chem. Soc.* **24** 802
82. Khan A 2003 *J. Chem. Phys.* **118** 1684
83. Beyer M K, Fox B S, Reinhard B M and Bondybey V E 2001 *J. Chem. Phys.* **115** 9288
84. Lee H M, Suh S B and Kim K S 2003 *J. Chem. Phys.* **119** 7685
85. Lee H M, Kim D and Kim K S 2002 *J. Chem. Phys.* **116** 5509
86. Lee H M and Kim K S 2001 *J. Chem. Phys.* **114** 4461
87. Kim J, Lee H M, Suh S B, Majumdar D and Kim K S 2000 *J. Chem. Phys.* **113** 5259
88. Majumdar D, Kim J and Kim K S 2000 *J. Chem. Phys.* **112** 101.
89. Baik J, Kim J, Majumdar D and Kim K S 1999 *J. Chem. Phys.* **110** 9116
90. Markovich G, Giniger R, Levin M and Cheshnovsky O 1991 *J. Chem. Phys.* **95** 9416
91. Markovich G, Pollack S, Giniger R and Cheshnovsky O 1994 *J. Chem. Phys.* **101** 9344
92. Combariza J E and Kestner N R 1994 *J. Phys. Chem.* **98** 3513
93. Xantheas S S and Dunning T H 1994 *J. Phys. Chem.* **98** 13489
94. Combariza J E, Kestner N R and Jortner J 1994 *J. Chem. Phys.* **100** 2851
95. Chen H Y and Shew W S 2000 *J. Am. Chem. Soc.* **122** 7534
96. Vanghn S J, Akhmatskaya E V, Vincent M A, Masters A J and Hillier I H 1999 *J. Chem. Phys.* **110** 4338
97. Kirkpatrick S, Gelatt C D and Vecchi M P 1983 *Science* **220** 671
98. Kirkpatrick S 1984 *J. Stat. Phys.* **34** 975
99. Car R and Parrinello M 1985 *Phys. Rev. Lett.* **55** 2471
100. Yockel S, Seals J J and Wilson A K 2004 *Chem. Phys. Lett.* **393** 448
101. Yu B, Li B, Sun P, Chen T, Jin Q, Ding D and Shi A C 2005 *J. Chem. Phys.* **123** 234902
102. Pan L, Li J and Wang L S 2008 *J. Chem. Phys.* **129** 024302
103. Xu M, Bacic Z and Hutson J M 2002 *J. Chem. Phys.* **117** 4777
104. Chaudhury P, Dutta P, Bandyopadhyay P, Sarkar P and Bhattaharyya S P 1996 *Chem. Phys. Lett.* **250** 238
105. Dutta P and Bhattaharyya S P 1990 *Chem. Phys. Lett.* **167** 309
106. Nandi S, Chaudhury P, Sharma R and Bhattaharyya S P 2008 *J. Theor. Comp. Chem.* **7** 977
107. Chaudhury P, Metzler R and Banik S K 2009 *J. Phys. A* **42** 335101
108. Guha S and Chaudhury P 2010 *J. Mol. Struct. (THEOHEM)* **945** 12
109. Guha S, Ray S and Chaudhury P 2011 *Struct. Chem.* **22** 1007
110. Guha S, Mukherjee N and Chaudhury P 2012 *Indian J. Phys.* **86** 245
111. Merrill G N and Webb S P 2003 *J. Phys. Chem.* **A107** 7852
112. Masamura M 2002 *J. Chem. Phys.* **117** 5257
113. Hermansson K, Bopp P A, Spaangberg D, Pejov L, Bako I and Mitev P D 2011 *Chem. Phys. Lett.* **514** 1
114. Wales D J and Walsh T R 1997 *J. Chem. Phys.* **106** 7193
115. Wales D J and Walsh T R 1996 *J. Chem. Phys.* **105** 6957
116. Wales D J and Ohmine I 1993 *J. Chem. Phys.* **98** 7257
117. Wales D J and Ohmine I 1993 *J. Chem. Phys.* **98** 7245
118. Kiss P T and Baranyai A 2009 *J. Chem. Phys.* **131** 204310
119. Bader R F W 1990 *Atoms in molecules a quantum theory* (Oxford, UK: Oxford University Press)
120. Koch U and Popelier P L A 1995 *J. Phys. Chem.* **99** 9747
121. Mani D and Arunan E 2013 *Chem. Phys. Chem.* **14** 754
122. Raghavendra B and Arunan E 2008 *Chem. Phys. Lett.* **467** 37
123. Aiswaryalakshmi P, Mani D and Arunan E 2013 *Inorg. Chem.* **52** 9153
124. Arunan E Desiraju G R, Klein R A, Sadlej J, Scheiner S, Alkorta I, Clary D C, Crabtree R H, Dannenberg J J, Hobza P, Kjaergaard H G, Legon A C, Mennucci B and Nesbitt D J 2011 *Pure. Appl. Chem.* **83** 1619
125. Arunan E and Mani D 2013 Phys. *Chem. Chem. Phys.* **15** 1537